Spatial and Temporal Coherence in a Long range, Upslope Environment

Theo Kooij

BBN Systems and Technologies, 1300 N. 17th Street, Arlington, VA 22209, USA

Theresa S. DeDominicis

Space and Naval Warfare Systems, Code PMW 183-52, Arlington, VA 20363-5200, USA

Abstract In an active acoustic test conducted off the USA Pacific Coast in November-December 1991, a low-frequency source, kept stationary over the deep basin, insonified from long range the coastal slope and shelf. An autonomous, bottom-mounted horizontal array was deployed at the transition from slope to shelf. The inter-hydrophone coherence along the array deteriorated with spacing, and the beamformer output exhibited a corresponding degradation in array signal gain. The coherences were measured after matched filtering of the received hyperbolic frequency-modulated signals. The spatial coherence is in strong contrast with the good temporal coherences for subsequent transmissions. The excellent measured temporal coherence is shown to have the potential to reduce the levels of direct arrivals and of reverberation.

1. Introduction

The Air Defense Initiative (ADI) is a program focusing on concept exploration for a system designed to defend the Continental United States (CONUS) against "air breathing" weapons systems. The scope of the original program has been expanded to include similar theaters worldwide. The problem entails Anti-Submarine Warfare (ASW) in a harsh acoustic environment that includes the deep basin, the slope and the shelf.

In the Fall of 1991, the ADI-ASW Program conducted a major at-sea experiment to explore several system concepts and the environmental effects of very low frequency (VLF) bottom interaction. The experiment was conducted in cooperation with the Critical Sea Test (CST) Program, and was known as the ADI-ASW E-1/CST-6 at-sea experiment, where E-1 designates the first environmental experiment for the program. The fundamental environmental issues examined during the experiment included transmission loss, the effects of spatial coherence on beamforming, and the effects of temporal coherence on reverberation reduction.

2. Test and Analysis Description

The experiment was conducted in November and December of 1991 off the northwest coast of the United States (Figure 1). The primary source platform for the experiment was the M/V CORY CHOUEST, outfitted with an array of fourteen coherent HLF6A hydro-acoustic sources (Figure 2), having an operating bandwidth greater than 100 Hz. The source platform was positioned at 46-50N 127-20W, approximately 185 kilometers from the continental slope, in the deep basin area, and was held stationary by the use of a dynamic positioning system, which had an nominal accuracy of less than 5 meters.

One of the measurement systems used during the experiment was a horizontal bottom-mounted array, positioned at 46-51N 124-53W, at the edge of the shelf region. This SEACAL array contained 18 hydrophones with a uniform spacing d_C. The SEACAL units had a programmable recording time of over thirty hours and were periodically retrieved to change batteries and data tapes. The data acquisition was all digital, via videotape recordings that were transcribed onto Exabyte tapes once the recording package was retrieved. A uniformly weighted beamformer over the full length of the array would have a broadside beamwidth around four degrees. See Figure 3 for a representative receiver beampattern.

2.1 Transmitter Parameters

The nominal depth of the transmitting array center was 195 meters; the ocean bottom depth at that location was 2700 meters. At the time of the measurements analyzed in this paper, elements 5, 7, 9, and 14 of the source were disabled; the resulting source beampattern was as shown in Figure 4. The narrow beamwidth caused no significant transmission loss, since only a few rays, launched horizontally, made it up to the shelf, as will be discussed shortly. Measurements of the transmit array tilt were not used to correct the actual beampattern, since that would only affect direct arrival and reverberation levels, and not significantly influence coherence results. The signals used for analysis were hyperbolic frequency-modulated (HFM) waveforms, of 20-second duration, and with a bandwidth of 80 Hz.

2.2 Receiver Parameters

The horizontal SEACAL array recorded data during the period 12/09/0200 to 12/10/1000 (32 hours). The reported depth at that position was 86 fathoms = 157 meters. However, the depth from digitized bathymetry is 230 meters. Comparison with bathymetry of higher accuracy has not yet been attempted.

The reported orientation of the horizontal SEACAL after deployment was 316 degrees true; this corresponds to a steering angle of 316 - 270 = 46 degrees from endfire. Inter-element delay measurements found an arrival angle of 53.8 degrees from endfire. This would imply a vertical arrival angle of arccos(cos53.8/cos46) = 32 degrees, which is quite possible as we'll see in Section 2.4.

Figure 5 shows the delays measured from correlation maxima for the full band, from one end of the array to the other. The differences with linear delays based on a plane-wave arrival from 306 degrees relative (or 270 degrees true, where the source was located) are small. The root mean squared difference was measured as 1 ms. This corresponds to an expected signal gain degradation (SGD) of approximately 0.5 dB. By applying an "empirical" beamformer, which uses the measured inter-element delays, a correspondingly lesser SGD can be expected, as we'll show in the section on results.

2.3 Processing Description

The 18 SEACAL elements were sampled at 3263 Hz, with a dynamic range of 14 bits or 84 dB. The 20-second long HFMs require 65k samples storage per channel; in addition, we require another 50 percent for the desired processing window of 10 seconds. To

reduce data storage requirements, the signals were first matched filtered before they were correlated. This causes an additional dependence on the signal spectral shape, which in this study was not removed by de-emphasis processing, as could have been done. For a broadband HFM, which dwells at lower frequencies longer than at the higher frequencies, the spectral emphasis can be considerable (more than 6 dB over the band in our case). The effect of this is discussed next.

In the following, we use frequency domain notation. Let S(f) be the transmitted signal; X(f) and Y(f) are signals received at hydrophones x and y. Let the ocean multipath response be $H_x(f)$ and $H_y(f)$ for hydrophone positions x and y. Then $X = H_x S$, and $Y = H_y S$.

Cross correlation of these two "raw" signals yields

$$G_{xy}(f) = X(f)\, Y^*(f) = H_x(f)\, H_y^*(f)\, |S(f)|^2 \qquad (1)$$

where the asterisk denotes complex conjugation. If the signals are first matched filtered, they take the form

$$Z_x(f) = S^*(f)\, X(f) = |S(f)|^2\, H_x(f) \qquad (2)$$

Correlation of such a pair of signals leads to

$$Z_x(f)\, Z_y^*(f) = H_x(f)\, H_y^*(f)\, |S(f)|^4 \qquad (3)$$

The difference between Eqs.(1) and (3), i.e., the difference between matched filtered and raw signal correlation, is the extra spectral emphasis, $|S(f)|^2$.

The implementation of the cross correlation algorithm is shown in Figures 6 and 7. The two-step procedure was chosen to be able to obtain a correlation coefficient of exactly unity in a relatively simple way. The signals to be correlated are chosen on a processing screen as "snippets," which are not necessarily of the same window size. A first correlation pass determines the most likely offset between the two snippets, from which the common window start is derived. Next, the window ends are cut off to create identical window sizes. The second correlation pass is then executed on the aligned and equal-windowed signals, and the maximum correlation will occur at zero relative offset. Absolute timing is kept track of, so that actual time differences can be measured.

2.4 Environmental Description

The unique feature of the E1 test configuration is the large stand-off range of the source in the deep ocean, the slope rising up from the ocean basin, and the shallow shelf with the water stretching out past the receiver toward the coast. The SEACAL array was positioned just at the crest of the sloping area and the shelf. See the diagram of Figure 8 for a profile of the ocean bottom. The steepest slope, according to the digitized bathymetry used, is 8 degrees, which is considerable for an ocean bottom slope; it occurs at 157 km (85 nmi) along the track. The Sound Speed Profile (SSP), shown on the left of Figure 8, was one of a set taken during an earlier TL run from the source towards the coast. The microchannel did not appear everywhere along that leg; however, its presence

or absence did not significantly affect the general character of the raytraces. The great-circle distance from stationary source platform to the bottomed receiver was 186.2 kilometers (100.55 nmi).

With the aid of the range-dependent ray trace program (BBN's SUNRAY), the peculiar character of the acoustic environment becomes evident from Figure 8. Only rays launched within a one-degree angle at the source have sufficiently few bottom bounces to arrive with worthwhile energy on the shelf. It is clearly seen that there are three CZ cycles, with the sound not touching the first rise from 111 to 148 km (60 to 80 nmi). However, at 166.7 km (90 nmi) from the source, rays hit the slope. Each bottom bounce increases the ray angle by twice the slope angle, so that, at the crest of the slope, the ray angle ends up to be greater than 30 degrees. This is way past any acceptable critical angle, and the bottom losses can be expected to be severe. In normal mode representation, the increase in ray angle is reflected in a corresponding decrease in forward propagation speed.

The ray trace diagram of Figure 9 shows, in the inset, a ray terminating at 189 km (102 nmi). At that range, the preset limit of a maximum of 20 bottom bounces has been reached. This anomalous ray, launched at 0.2 degree, is seen to hit the upslope early, at 163 km (88 nmi), where the bottom slope is 4.5 degrees, with the result that the ray arrives on the shelf with a much steeper angle than the other rays in the fan (from -0.4 to +0.6 degrees). Consequently, the anomalous ray dies out quickly after little progress, while the others continue out to 192.6 km (104 nmi).

3. Test Results

The test signals were transmitted according to a 0:00 - 3:00 - 12:00 - 15:00 minute schedule, i.e., two signals separated by three minutes, with a gap of nine minutes between pairs. During the gap, signals in a different band were transmitted, which are not analyzed here. The combination of array element recordings of successive pings, for a fixed configuration, made it possible to investigate both spatial and temporal coherence. The direction of the source relative to the receiver was 46 degrees from array endfire. Although this configuration covers neither pure transversal, nor pure longitudinal spatial incidence, it allows a look at coherence for both situations in a single measurement setup.

Although the word "coherence" has been used freely, it is used here in the generic sense of the similarity of two signals when processed in a "coherent" way. The goal is to improve the detection index or signal to noise ratio. This is done by "coherently" adding signals to obtain an linear increase of their amplitudes, while the noise or interference hopefully adds only as incoherent power. This way, the well known 20 log(M) signal gain and the 10 log(M) noise gain are obtained, where M is the number of observations. In the case of an array, the difference between signal and noise gains is, of course, the array gain over M elements. In this paper, the "coherence" measurements should technically be called correlation function, correlation coefficient, or (the maximum of) the correlation coefficient function. See Bendat and Piersol[1] for appropriate definitions. The correlation coefficient used in this paper is linear $\{\rho = C_{xy}/(\sigma_x\sigma_y)\}$, not the squared version ρ^2. The advantage of the linear form is that it is possible to discern negative

correlations, which may occur when bandshifted or bandlimited signals, which contain a distinct carrier frequency, are considered.

3.1 Raw Signals

Figure 10 shows a linear waterfall plot of the raw signals for the first ping, which was transmitted at 2:00 hrs and arrived 2 minutes and 4 seconds later. Note the signal duration of 20 seconds, and the different interference pattern of the signals received along the array. This variation in the waveforms is the result of spatially different structure of the multipaths, which will become even more apparent after matched filtering or pulse compressing the raw waveforms. As shown, the waveforms already illustrate the dependence of the transmission loss function both on frequency and on spatial location of the receiving hydrophone.

Signals 2, 3, and 4 show a low frequency vibration independent of the sonar signal. This 2 Hz interference seems to be due to strum near these particular hydrophones, from which one might conclude that this part of the bottom mounted array is probably suspended freely above the bottom. The matched filtering removes this out-of-band noise completely. The signal from element 15 appears weaker; this could be because of hydrophone sensitivity, which was not recalibrated, or because of some shielding effect at that hydrophone location. Subsequent pings showed a very similar overall behavior.

3.2 Matched Filtered Signals

Figure 11 shows a waterfall plot of the matched filtered signals of the first ping, again on a linear scale. The strum has disappeared, element 15 is still weaker, but looks coherent with its immediate neighbors. We see that the overall received level along the array decreases with the distance from the first phone, as could be seen already in the raw signals of Figure 10. The first half of the array shows for each trace two arrivals, about 62 msec apart. Near the tail end of the array, this pair of arrivals fades, and an interstitial pair appears. There is no doubt that this variation along the array is the result of local bottom and sub-bottom scattering effects[2], and not of some long-range longitudinal propagation effect (such as a path exchange, in raytrace language). Figure 12 shows a similar plot for ping 3, which was sent 12 minutes later. Overlaying both plots shows a remarkable coherence between the two sets of signals, which will become quantitatively apparent when we perform the temporal cross correlation.

3.3 Correlation Coefficient Functions

Figures 13 and 14 show the cross correlation coefficient functions for the first ping at hydrophones 1 and 12, using raw and matched filtered waveforms, respectively. The correlations differ somewhat, but their maximum values are close, 48 versus 49 percent. The extreme value appears to have "jumped" within the envelope from the third fine-structure cycle to the negative one-and-a-half cycle, with attending negative correlation coefficient. In Section 2.3, the difference between raw and matched filtered processing was discussed to explain the difference in cross correlation functions. As shown here, the difference is real, but not great.

3.4 Maximum Correlation Coefficients

Figure 15 shows a plot of the maximum correlation coefficients for pings 1 and 2, for the full signal band (80 Hz). The signals are the matched filtered direct arrivals. One pair of curves is for the maximum correlations of all elements against the first element, the other pair of curves is for the maximum correlations against the last element, number 18. One can consider these curves as the first and last rows of an 18X18 correlation coefficient matrix, $\langle \underline{x}(t)\underline{x}^T(t-\tau_{max})\rangle$, where the superscript "T" denotes transpose, the brackets indicate time average, and $\underline{x}$ is a (column) vector of signals, so that $\underline{x}^T = \{x_1(t), x_2(t), ..., x_M(t)\}$. The elements of the matrix are normalized by the square roots of energies of the contributing signals. The coefficient curves show a relative minimum, whether the reference signal was chosen at one end of the array or at the other end. This is different from the characteristic behavior of coherence obtained from other measurements[3,4], which generally show a monotonically decreasing curve as a function of L/λ. In our case, the array length is $L = 12.2\ \lambda$.

3.5 Signal Gain Degradation

A delay-and-sum beamformer adds up the signals from all elements, after appropriate delays. The delays can be derived from assumed element spacings, sound speed, and desired steering angle, or from the actual element locations, if known, or they could be determined from the actual delay measurements. Assuming that all signals have been delayed to maximum coincidence or coherence with each other, the signal part of the beamformer output y is the sum of M time signals, $y = \{x_1(t-\tau_{max}) + x_2(t-\tau_{max}) + ... + x_M(t-\tau_{max})\}$. Squaring this sum can be considered to be the same as taking the sum of all elements of the maximum correlation matrix, $\langle \underline{x}(t)\underline{x}^T(t-\tau_{max})\rangle$, as described above in Section 3.4. Since the elements of this matrix can be derived directly from the normalized values by multiplying back the element signal energy levels, we can theoretically reconstruct the maximum beamformer output. See Urick[5] for further details on signal gain and correlation.

If all signals were perfectly coherent, all maximum cross correlation coefficients would be equal to unity. By comparing this ideal beamformer output with the theoretically derived value, the expected theoretical signal gain degradation is found. The theoretical beamformer output should actually be calculated from addition of all elements of the correlation matrix. In our case, so as not to have to calculate the whole matrix, it is assumed to be a circulant, either based on the measured correlations referenced to hydrophone 1 ("first row coherence"), or referenced to hydrophone 18 ("last row coherence"). The dB average of these two results is taken as an estimate of the theoretical beamformer output.

Finally, the actual beamformer can be implemented and its output energy determined (over the same time window as for the elements at the beamformer input). Table 1 shows the output values of the ideal beamformer (based on unity correlations and measured element levels), of the theoretical beamformer (based on the measured correlations and element levels), of the empirical beamformer (based on the measured maximum correlation delays), and of a traditional beamformer (based on calculated delays of a straight array) steered at the maximum response angle (in our case, 306 degrees relative).

TABLE 1 - Ideal, Theoretical, and Measured Beamformer Outputs (dB)

	Ping 2:02	Ping 2:05	Ping 2:14	Average
Average Energy	0.53	0.43	0.41	0.46
Ideal Beamforming	0.02	-0.08	0.06	0.00
First Row Coherence	-0.80	-0.97	-0.83	-0.87
Last Row Coherence	-1.18	-1.63	-1.26	-1.36
Average Theor. BF	-0.99	-1.30	-1.05	-1.11
Empirical BF	-1.30	-1.52	-1.30	-1.37
Straight Array BF	-1.70	-1.93	-1.51	-1.71

The Table has been biased so that the dB average of the ideal beamformer outputs equals zero dB. Added is a row of the power averages for the signal energy of each hydrophone. This average input energy is greater than the output of the ideal beamformer, since the average of squares is greater than the square of the average, except when all terms are equal.

Note that the SGD of the straight array beamformer is only 0.3 dB worse than the SGD of the exact, empirical beamformer. In Section 2.2 we had expected 0.5 dB, based on the deviations of the measured delays. The SGD of the empirical beamformer (1.37 dB), is practically the same as that of the calculated theoretical beamformer (1.11 dB). This value can be taken as the SGD as a result of decorrelation of the signal along the receiver.

3.6 Temporal Coherence

We showed earlier that successive transmissions resulted in extremely similar arrival structures of the matched filtered sound received on the horizontal array. The maximum correlation coefficients are given in Table 2, for hydrophone numbers 1, 5, 9, 13, and 17.

TABLE 2 - Temporal Correlation Coefficients and Delays

Ping Pair hr:min	Time Diff. sec	Meas.Delay sec	Range Shift m	Av. Corr. Coeff.
02:02-05	180	180.0007	1.2	0.972
02:02-14	720	719.9918	-12.3	0.939
02:02-17	900	899.9892	-16.2	0.967

One result that follows from the temporal measurements is the delay between maximum correlations. Since the signals were transmitted starting exactly on the minute, an absolutely fixed configuration would have resulted in arrivals an integer number of minutes apart. However, from Table 2 it follows that the deviations reach as much as 10.8 milliseconds, which corrresponds to approximately 16.2 m. This is more than the nominal 5 m of the specification for the source positioning system.

The stability of the ocean environment when a fixed configuration is maintained has been shown before[6]. The advantage of measuring the temporal correlation coefficient is that it

allows one to make a quantitative prediction of the attainable reduction in the direct blast or reverberation level, as explained in the next Section.

3.7 Direct Blast Reduction

The relatively high temporal coherence has implications for the amount of direct blast or reverberation reduction obtainable, provided the source to receiver geometry does not change. If the correlation coefficient is based on signal-to-noise ratio alone, it is simple to show that, with

$$\rho = \langle (s+n_1)*(s+n_2)\rangle / \ (\sqrt{\langle (s+n_1)^2\rangle * \langle (s+n_2)^2\rangle} \tag{4}$$

we obtain

$$\rho = SNR / (SNR + 1) \tag{5}$$

where SNR is the signal-to-noise ratio, $\langle s^2\rangle / \langle n^2\rangle$

The squared difference between the two signals, normalized by the averaged signal plus noise power (assumed to be equal for the two inputs), becomes

$$NSD = \langle |(s+n_1)-(s+n_2)|^2\rangle / (\langle s^2\rangle + \langle n^2\rangle) = 2 / (SNR+1) \tag{6}$$

where NSD stands for Normalized Squared Difference. This quantity indicates the reduction in level that can be attained when two noisy signals are subtracted from each other. Eliminating SNR from Eq.(5) and Eq.(6), one obtains an expression of the NSD in terms of coherence:

$$NSD = 2\ (1-\rho) \tag{7}$$

It follows that a correlation coefficient of 0.95 implies an NSD of 0.1, or -10 dB. The attainable suppressions, based on the measured correlation values of Table 2 are -12.5, -9.1, and -11.8 dB, respectively. See Table 3 for other values of potential reduction versus coherence.

TABLE 3 - Signal Suppression as Function of Coherence

SNR [dB]	rho (coherence)	NSD (suppression) [dB]
0	0.5	0
3	0.67	-1.75
6	0.8	-4.0
10	0.9	-7.4
20	0.99	-17
30	0.999	-27
40	0.9999	-37

A more general expression[7], based on N observations to estimate the coherent part of the (N+1) input, leads to a potential reduction equal to

$$NSD = (N+1)(1-\rho) / N \qquad (8)$$

This performance is independent of how the reduction is implemented.

4. Conclusion

Measurements of spatial and temporal coherence indicate that even under the difficult environmental conditions that prevail when the shallow coastal shelf region is insonified from a stand-off source in the ocean basin, both spatial and temporal coherence show that linear beamforming suffers only limited loss. The decorrelation along the array was modest, reaching just below 0.5 within the array aperture. The corresponding signal gain degradation is small, just over 1 dB, and can be derived directly from the correlation matrix by the standard methods. The temporal stability was shown to be excellent (0.94 to 0.97), which would allow signal suppression performance of more than 10 dB.

References

[1] Bendat, J.S., and Piersol, A.G., *Engineering Applications of Correlation and Spectral Analysis*, Wiley-Interscience, New York, 1980, 43-56.

[2] Parvulescu, A., *Signal Correlation along Line Arrays*. Private Communication.

[3] Scholz, B., Horizontal Spatial Coherence Measurements with Explosives and CW -Sources in Shallow Water, *Aspects of Signal Processing*, G. Tacconi (ed.), Reidel, Dordrecht-Holland, 1977, 95-108.

[4] Cable, P., Marshall, W., Skarda, G., and Waldman, K., *Acoustic Characterization of a Shallow Water Site*, (This Volume).

[5] Urick, R.J., *Principles of Underwater Sound*, McGraw-Hill, New York, 1975, 36.

[6] Parvulescu, A., and Clay, C.S., Reproducibility of Signal Transmissions in the Ocean, Proc.of the Symposium Processing in Radar and Sonar Directional Systems: Paper No.26, Radio and El.Eng., Vol.29, No.4, April 1965.

[7] Grimmett, D., and Zabal, X., *Performance Criteria for Inter-Ping Reverberation Suppression Techniques*, NRaD Technical Report, In Preparation.

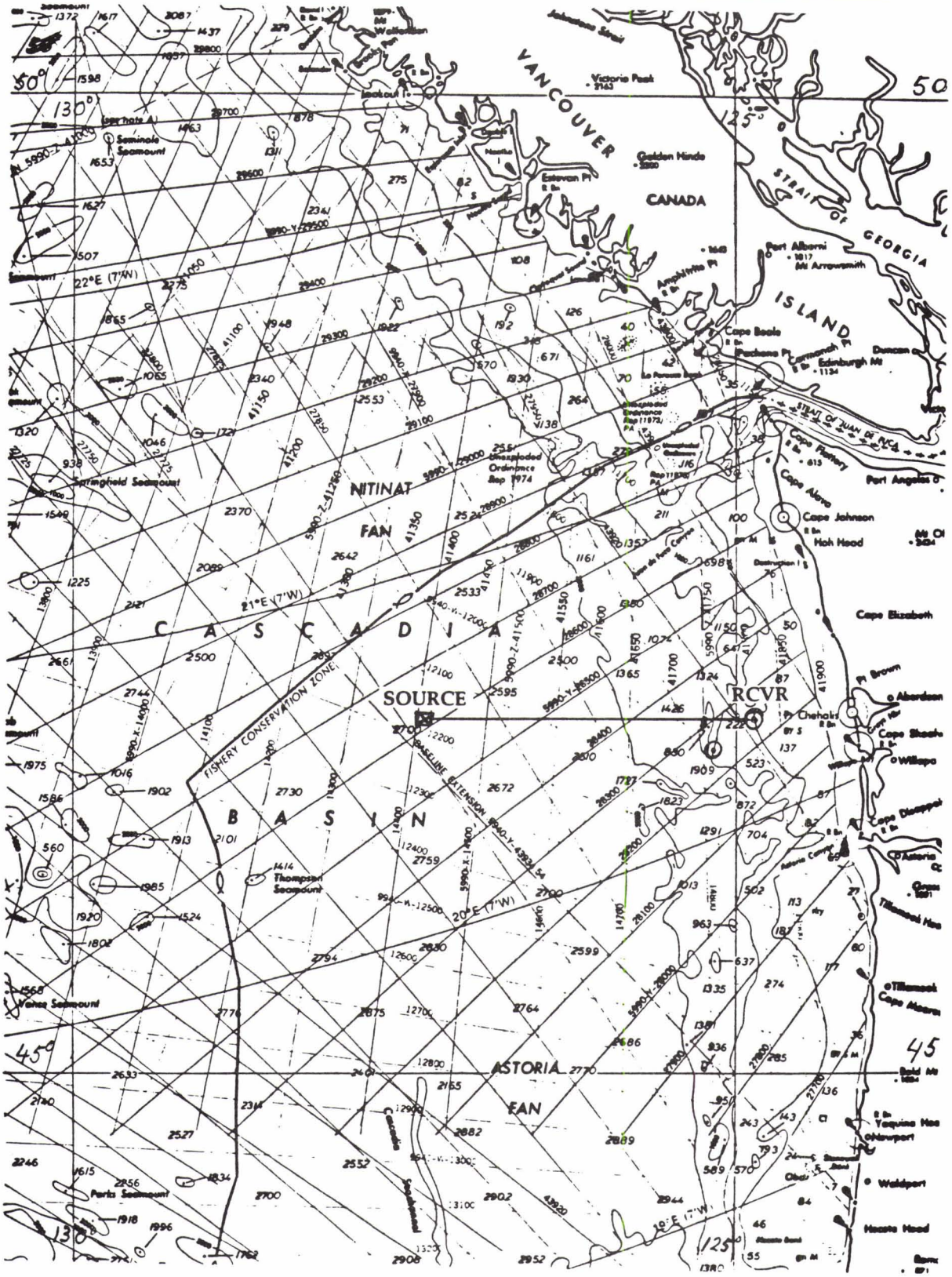

Figure 1. Test Area With Source And Receiver Locations

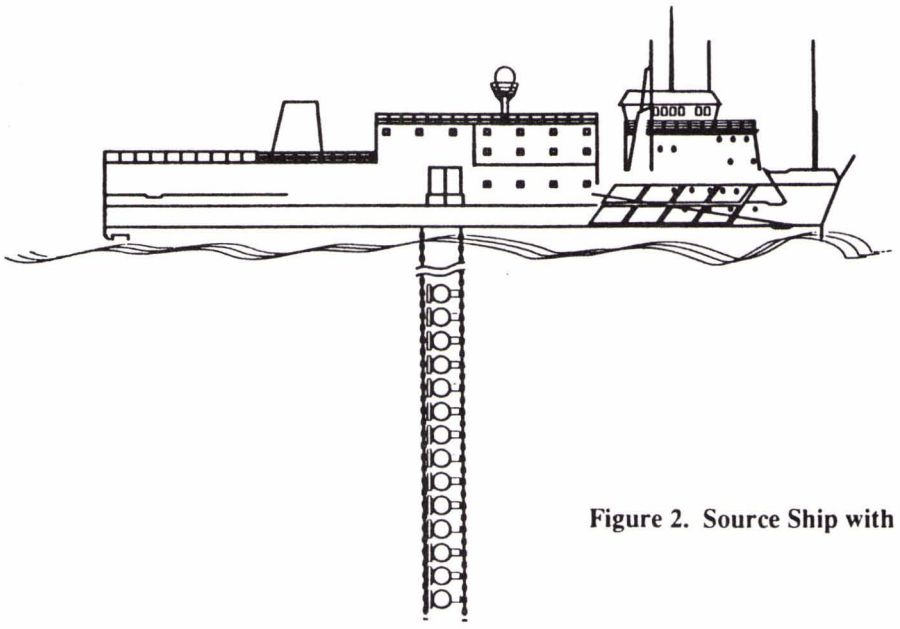

Figure 2. Source Ship with Vertical Array

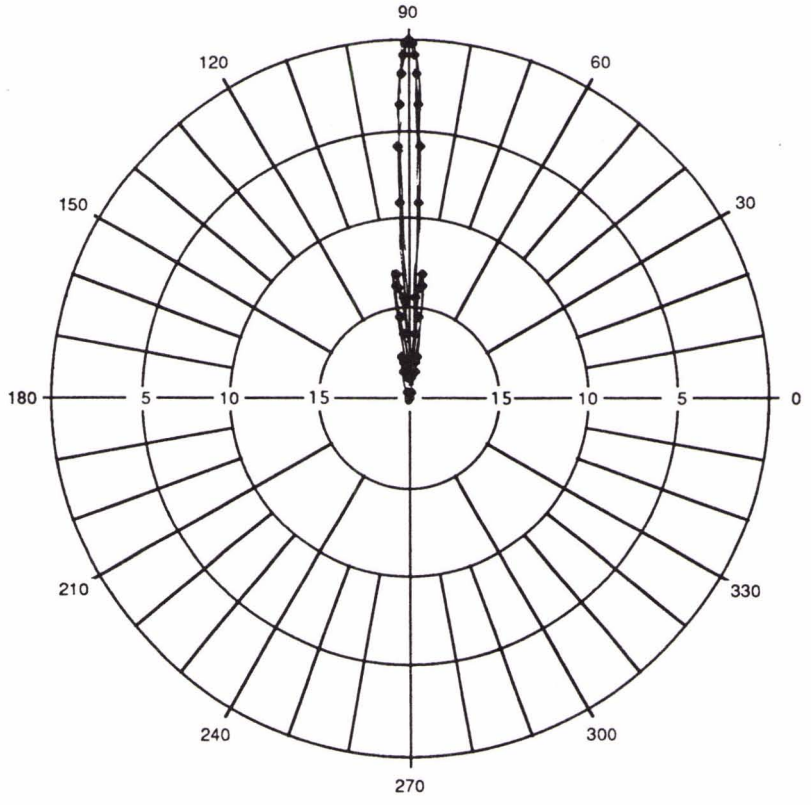

Figure 3. SEACAL Beampattern for Uniform Weighting

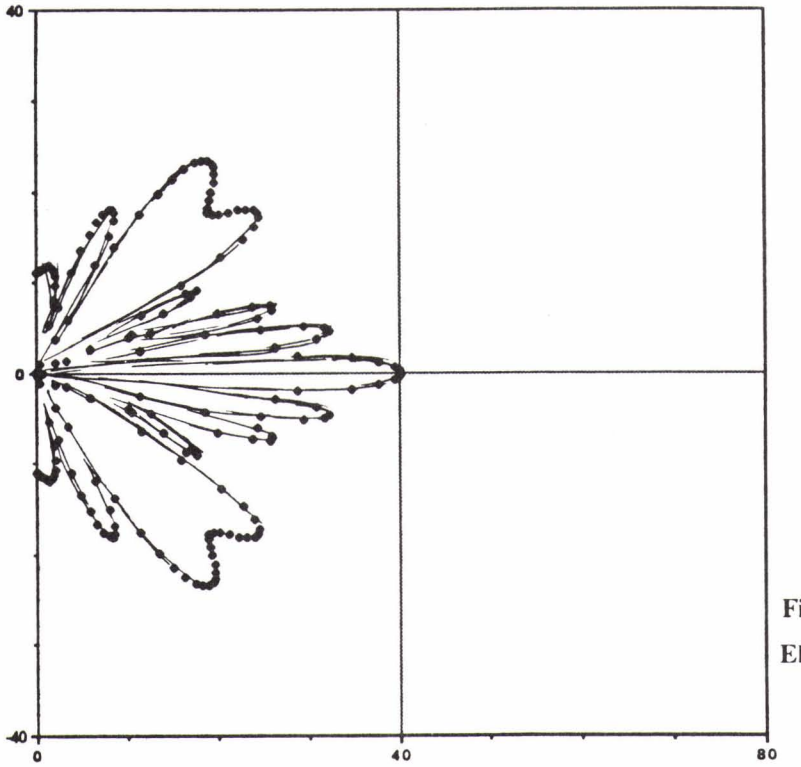

Figure 4. Source Beampattern, Elements 5, 7, 9, and 14 Disabled

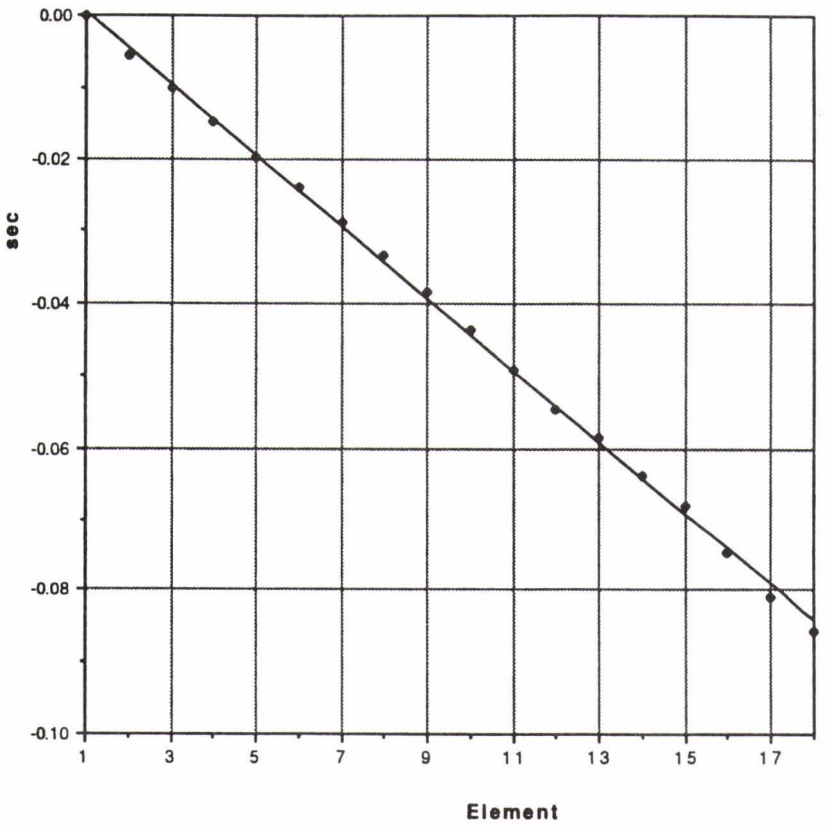

Figure 5. Inter-Element Delays for Direct Arrival

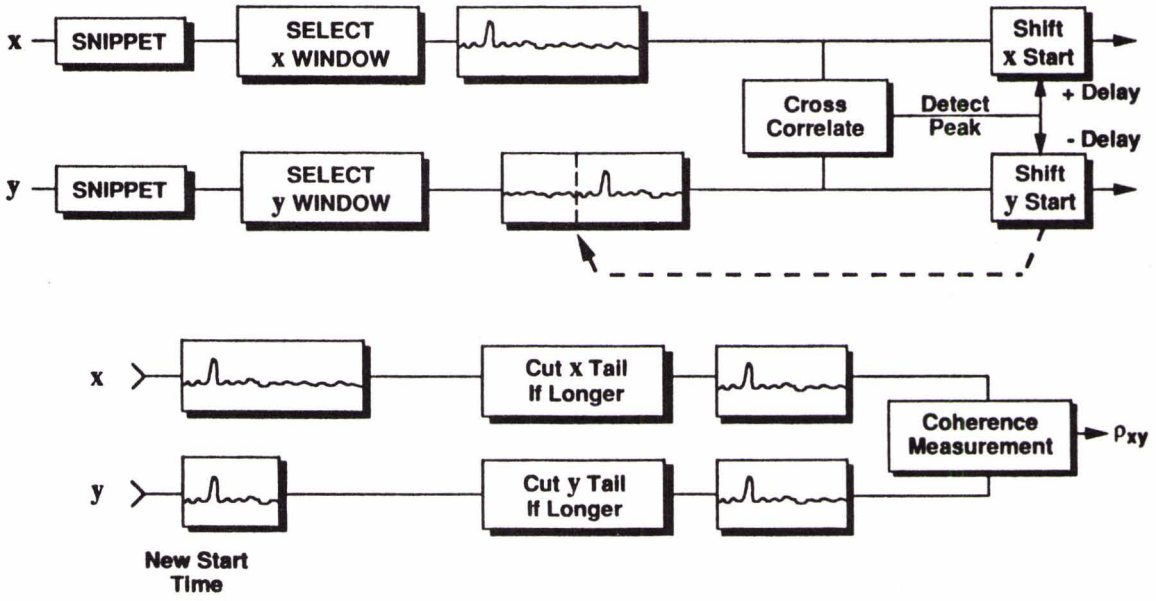

Figure 6. Two-Pass Coherence Measurement Diagram

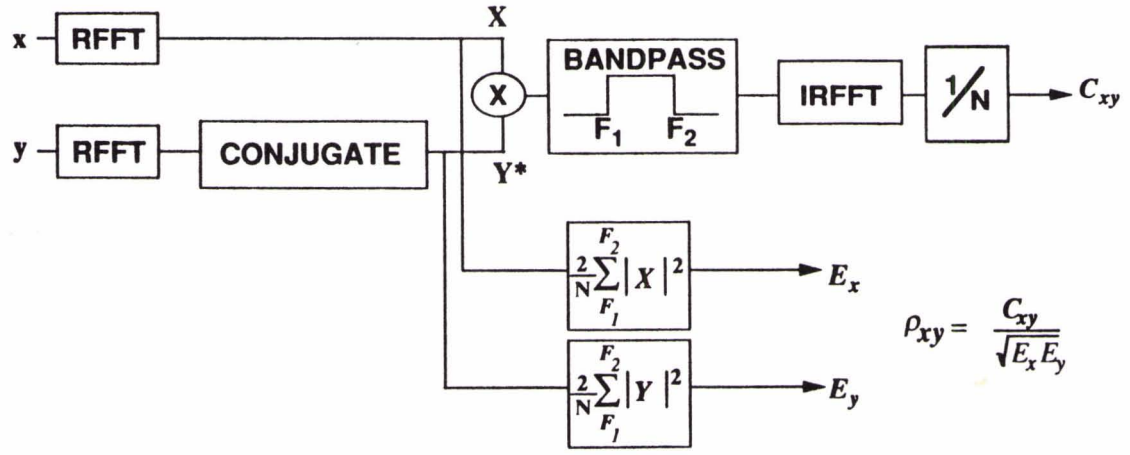

Figure 7. Correlation Coefficient Function Algorithm

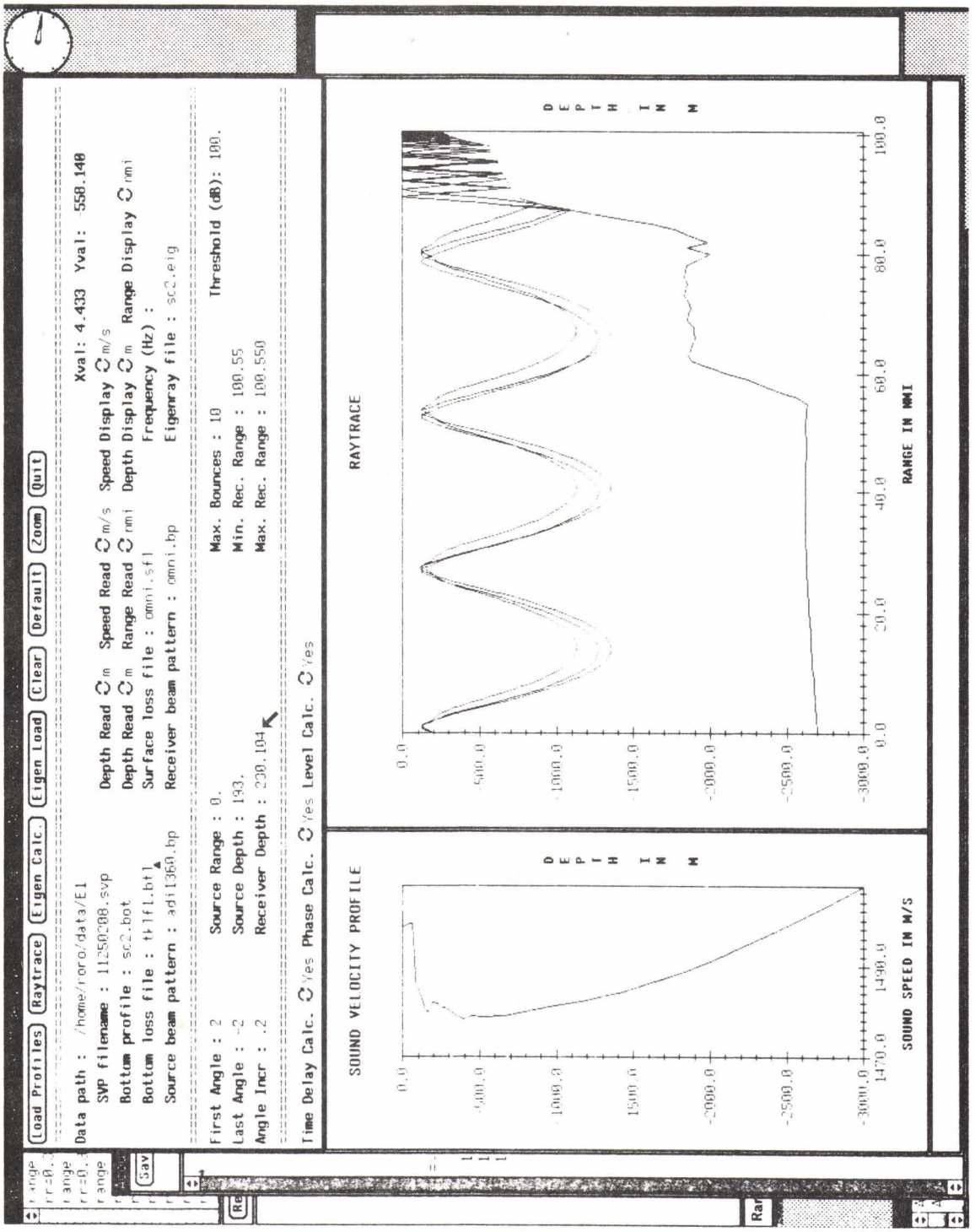

Figure 8. BBN SUNRAY Diagram, with SSP and Bottom Profile

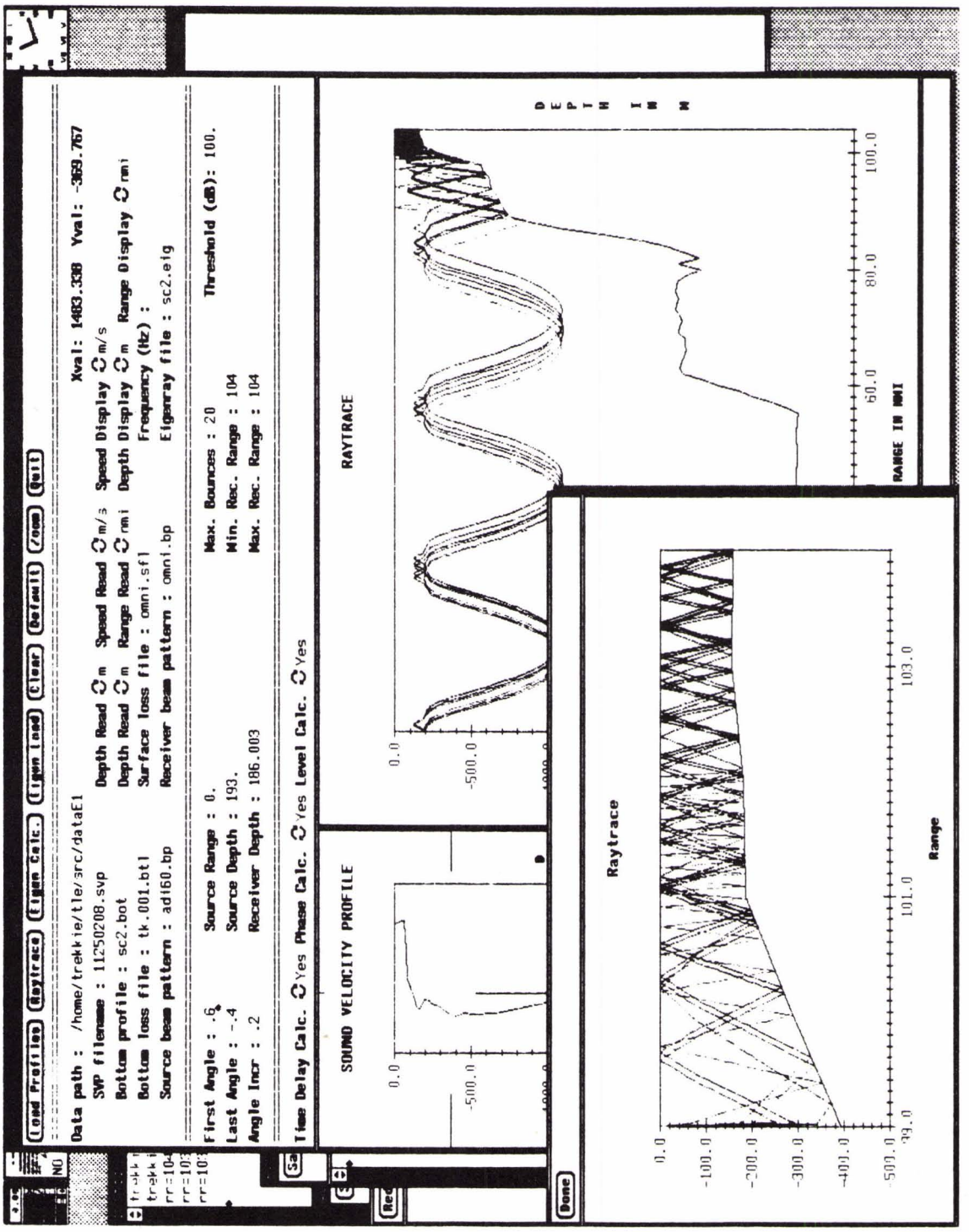

Figure 9. Ray Diagram for Slope-to-Shelf Transition

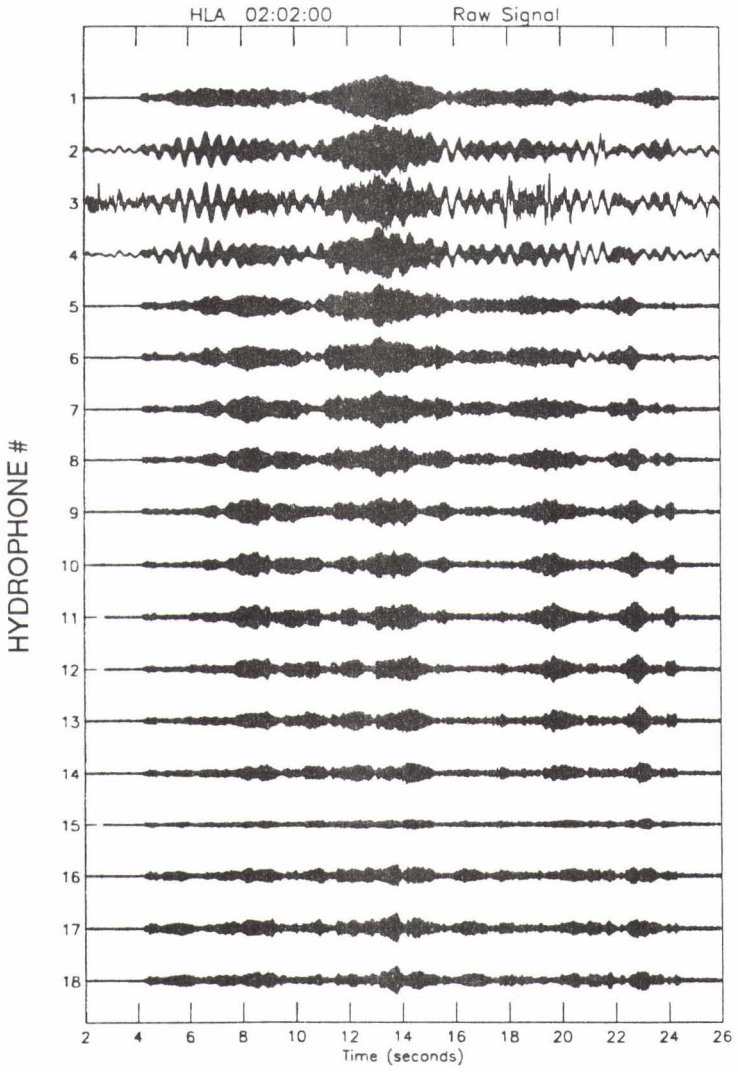

Figure 10. Waterfall Display of Unprocessed Hydrophone Signals, Time 02:02

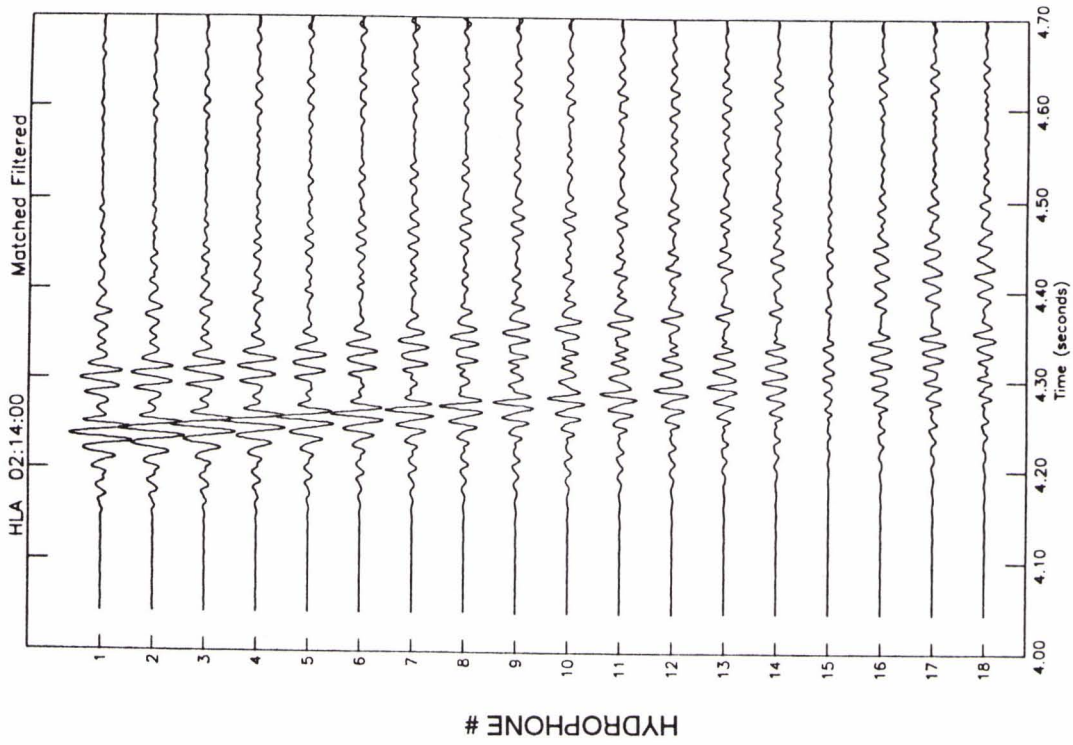

Figure 12. Waterfall Display of Matched Filtered Hydrophone Signals, Time 02:14

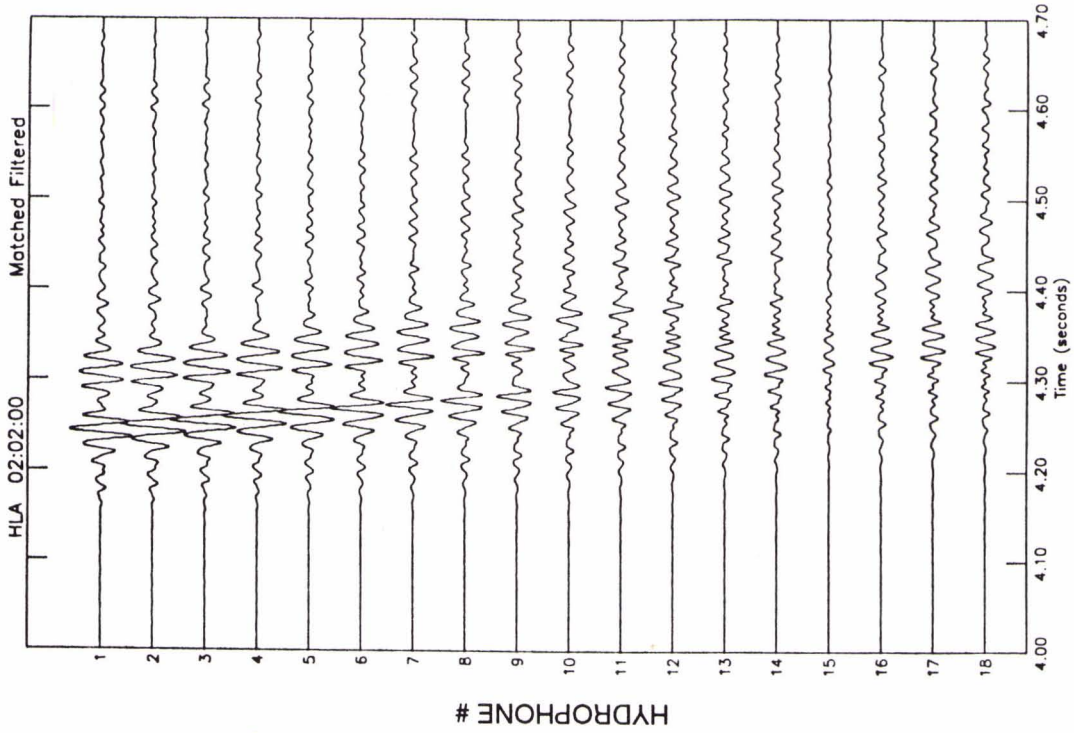

Figure 11. Waterfall Display of Matched Filtered Hydrophone Signals, Time 02:02

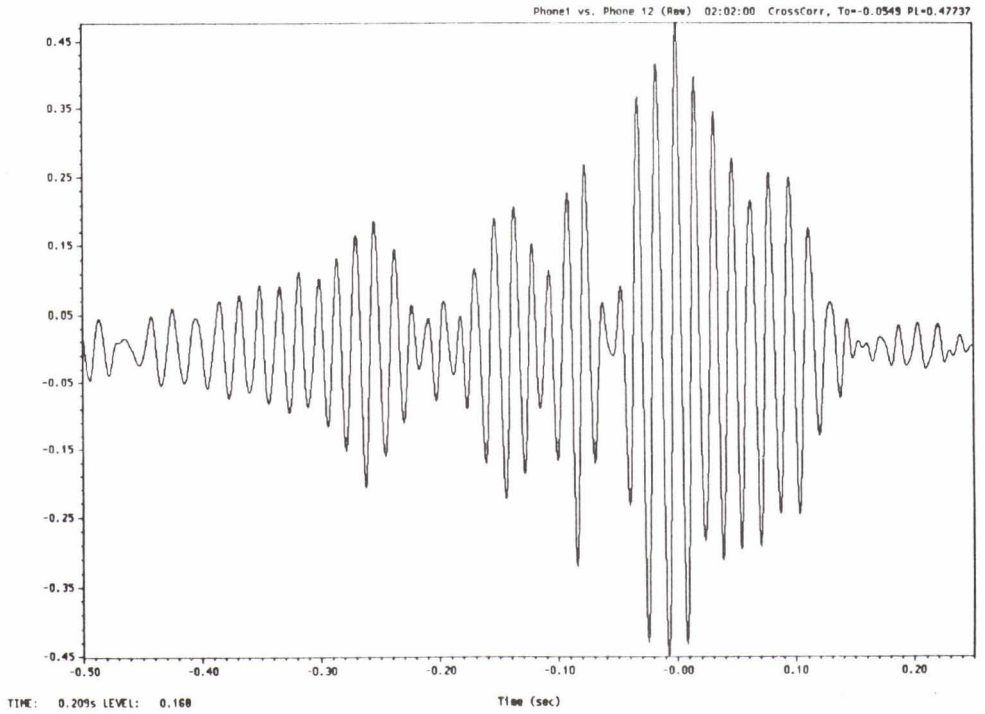

Figure 13. Correlation Coefficient Function for Unprocessed Hydrophones 1 and 12

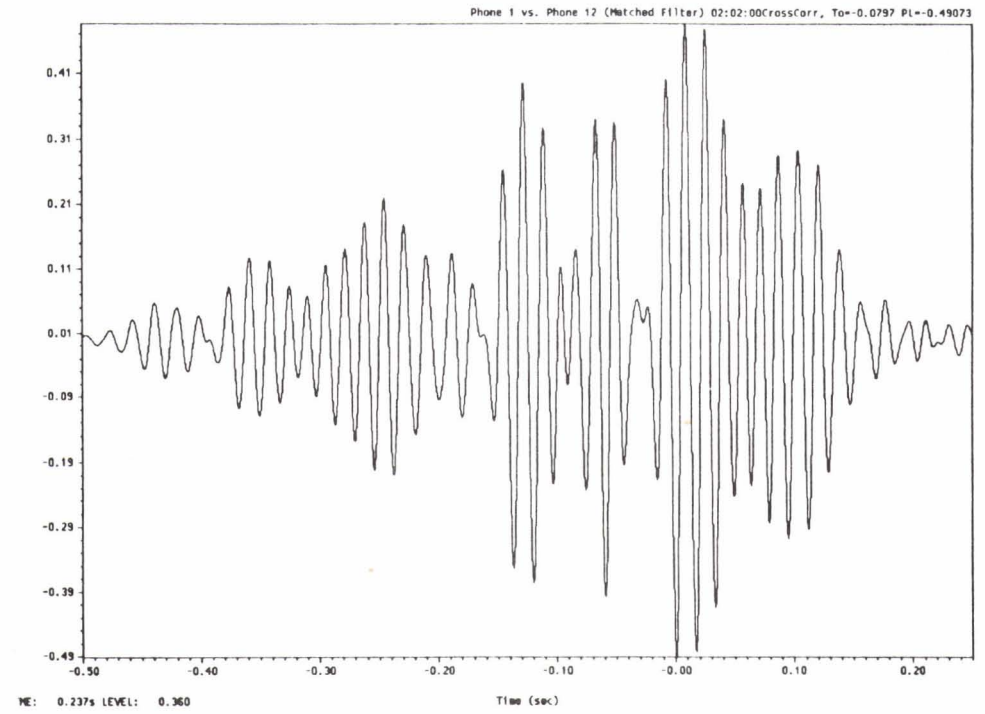

Figure 14. Correlation Coefficient Function for Matched Filtered Hydrophones 1 and 12

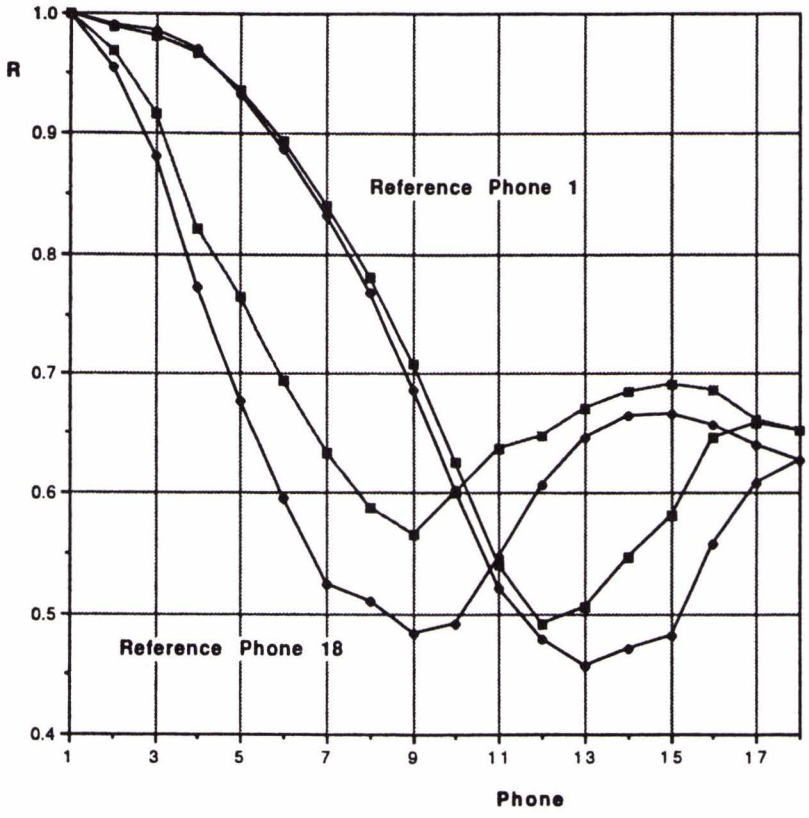

Figure 15. Maximum Correlation Coefficients Referenced to Array Ends; Times 02:02 and 02:05